Journal of Materials Chemistry A

Accepted Manuscript

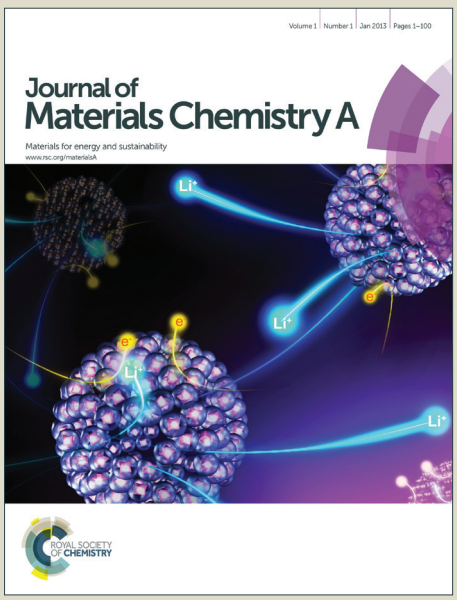

ROYAL SOCIETY OF CHEMISTRY

www.rsc.org/materialsA

Table of Contents Entry

Ionothermal synthesis of black Ti^{3+}-doped single-crystal TiO_2 as an active photocatalyst for pollutant degradation and H_2 generation

Guisheng Li[1], Zichao Lian[1], Xin Li[1], Wenchao Wang[1], Dieqing Zhang[1], Fenghui Tian[2], Hexing Li[3*]*

1. Chinese Education Ministry Key Laboratory of Resource Chemistry, Shanghai Normal University, Shanghai 200234, China. Email: liguisheng@shnu.edu.cn. 2. Institute of Computational Science and Engineering, Qingdao University, Qingdao, 266071, China. 3. Shanghai University of Electric Power, Shanghai 200090, China. Email: Hexing-Li@shnu.edu.cn.

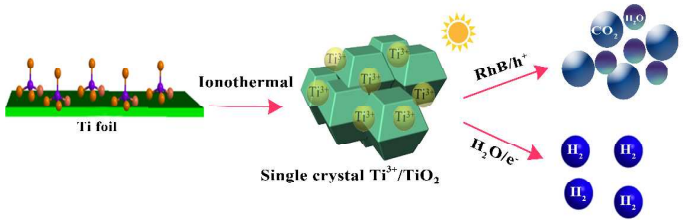

Black Ti^{3+}/TiO_2 single-crystals synthesized *via* an ionothermal process exhibited high activity for photocatalytic degradation of pollutants and hydrogen evolution reaction.

Ionothermal synthesis of black Ti^{3+}-doped single-crystal TiO_2 as an active photocatalyst for pollutant degradation and H_2 generation

Guisheng Li[1], Zichao Lian[1], Xin Li[1], Yuanyuan Xu[1], Wenchao Wang[1], Dieqing Zhang[1], Fenghui Tian[2], Hexing Li[3*]*

1. Chinese Education Ministry Key Laboratory of Resource Chemistry, Shanghai Normal University, Shanghai 200234, China. Email: liguisheng@shnu.edu.cn. 2. Institute of Computational Science and Engineering, Qingdao University, Qingdao, 266071, China. 3. Shanghai University of Electric Power, Shanghai 200090, China. Email: Hexing-Li@shnu.edu.cn.

Abstract

A black Ti^{3+}-doped single-crystal TiO_2 (Ti^{3+}/TiO_2) was one-pot synthesized by treating metal Ti in an ionic liquid containing LiAc and HAc under mild ionothermal conditions. The ionic liquid (1-methyl-imidazolium tetrafluoroborate) supplied an environment enriched with fluoride ions for dissolving titanium foil at ionothermal condition, followed by reducing protons in acetic acid to form Ti^{3+} ions, leading to Ti^{3+}-doped single-crystal TiO_2 in black powder. EPR and XPS results indicated the high-concentrations of both Ti^{3+}-dopants and oxygen vacancies. The Ti^{3+} incorporated into TiO_2 lattice could narrow the energy band gap of TiO_2 *via* forming intermediate energy levels, leading to the visible photocatalyst. Meanwhile, the oxygen vacancies could inhibit the photoelectron-hole recombination. As expected, such a black Ti^{3+}/TiO_2 exhibited high activity in photocatalytic degradation of organic pollutants and water splitting for H_2 production under irradiation with visible lights and/or simulated solar lights.

Keywords: Black Ti^{3+}-doped single-crystal TiO_2 (Ti^{3+}/TiO_2), ionothermal synthesis, visible photocatalyst, pollutant degradation and H_2 generation

Introduction:

TiO_2 photocatalyst has received more and more attentions in environmental cleaning and green energy production owing to its high activity, non-toxicity, easy availability, and strong stability for degradation of organic pollutants[1], H_2 production *via* water splitting[2] and direct photoelectric transformation.[3] Since the report of Fujishima and Honda in 1972[4], TiO_2-based

photocatalysts have been widely investigated in designing new photocatalysts, exploring fundamental theory and putting into practical applications. However, the application of pure TiO_2 photocatalyst is still quite limited since it can be activated by only UV lights due to the big energy band gap (anatase with a band-gap of 3.2 eV and rutile with a band-gap of 3.0 eV), taking into account that the sunlight contain large proportion of visible lights and very little fraction of UV lights. In the past two decades, cation-doping[5, 6], metal hybrid[7], semiconductor-doping[8], and nonmetal-doping ect.[5, 6] have been widely used to modify the electronic structure and consequently the light absorption range of TiO_2 for achieving visible photocatalysts in which there were using many methods to synthesis visible-light-driven-materials[9, 10], such as ionothermal method which could prepare TiO_2[11] and other materials[12, 13]. In addition, Also changing the morphology[14], preparing TiO_2-based[15] or doped composite[16] and enhancing (001) facet exposure rate[17-20] of TiO_2 would be increasing the photocatalytic activity.

Recently, both the experimental results and theoretical prediction demonstrate that the Ti^{3+}-doped TiO_2 with great number of oxygen vacancies (Ti^{3+}/TiO_2) usually displays black color[21] and strong spectral response in visible area.[22] Up to now, a variety of methods have been developed for synthesizing black Ti^{3+}/TiO_2, such as hydrogen reduction of TiO_2 at high calcination temperature and pressure,[23,24] high temperature induced molten aluminum reduction of TiO_2 etc.[25] Besides the harsh conditions and tedious experimental steps, these reported black Ti^{3+}/TiO_2 samples usually exhibited low photocatalytic activity under visible light irradiation due to the low-content of Ti^{3+}-dopants and the poor stability of Ti^{3+}-dopants against oxidation. Herein, a facile one-step approach was developed for synthesizing black Ti^{3+}-doped anatase TiO_2 single-crystal (Ti^{3+}/TiO_2) by treating Ti foil in 1-methyl-imidazolium tetrafluoroborate ionic liquid containing acetic acid (HAc), N-N dimethylformamide (DMF), and lithium acetate (LiAc) under 200 ^{o}C ionothermal conditions. The as-formed black Ti^{3+}/TiO_2 photocatalyst contained high-contents of Ti^{3+}-dopants and oxygen vacancies. The Ti^{3+}-dopants in the TiO_2 lattice could narrow energy band gap of TiO_2 semiconductor *via* forming intermediate energy levels, leading to the visible photocatalyst. Meanwhile, the oxygen vacancies could diminish the photoelectron-hole recombination and thus, could enhance the quantum efficiency of photocatalysis. As expected, this black Ti^{3+}/TiO_2 exhibited high activity in photocatalytic degradation of organic pollutants and water-splitting for H_2 generation under irradiation with visible lights and/or simulated solar lights.

Experiments

Catalyst preparation

All chemicals were analytical grade and used as received without any further purification. In a typical run of synthesis, 12 mL DMF (as solvent), 0.6 g $LiAc{\cdot}2H_2O$ and 18 mL glacial HAc (as buffer solution) were mixed in a 100-mL pyrex beaker and magnetically stirred for 15 min to get a clear solution. The mixture was then transferred to an autoclave (50 mL). Meanwhile, a piece of Ti foil (99.5 %, 20 mm*33 mm*0.3 mm) was ultrasonically cleaned in a mixed solution of deionized water, acetone, and ethanol with volume ratios of 1:1:1, followed by adding into the autoclave together with 2 mL ionic liquid (1-methyl-imidazolium tetrafluoroborate). The mixture was kept at 200^{o}C for 24 h and then, the black product was washed with water and ethanol for three times, followed by drying at 80 ^{o}C for 12 h.

Characterizations

X-ray diffraction (XRD) patterns were collected on a Rigacu Dmax-3C with Cu Kα radiation. Selected area electron diffraction (SAED) images and transmission electronic microscopy (TEM) morphologies were recorded on a JEM-2010. Field emission scanning electron microscopy (FESEM) images were performed on a JEOL JSM-6380LV. Raman spectra and UV-vis diffuse reflectance spectra (UV-vis DRS) were conducted on Dilor Super LabRam II and MC-2530 instruments, respectively. For expelling the local heating effect, same laser source (wavelength = 633 nm) was utilized in the Raman characterization for all samples. The photoluminescence spectroscopy (PLS) was collected on Varian Cary-Eclipse 500 excited with 280 nm lights. The photocurrent responses in the light on-off process were determined in a homemade three electrode quartz cell containing 0.5 mol/L Na_2SO_4 aqueous solution under visible lights (> 420 nm) irradiation at an applied potential of 0.5 V vs. SCE with electrochemical workstation (CHI 660D, Chen Hua Instrument Co., Ltd.). X-ray photoelectron spectroscopy (XPS) analysis was performed on a Perkin-Elmer PHI 5000C ESCA system. All binding energies were calibrated by using the contaminant carbon (C_{1s} =284.6 eV) as a reference. Thermogravimetric analysis (TG) were carried out on a DTG-60H thermogravimetric analyzer with a heating speed of 10 °C/min under air atmosphere. The electron paramagnetic resonance (EPR) spectra were recorded at 100 K using a

Bruker EMX-8/2.7 EPR spectrometer. Solid state ^{1}HNMR was recorded on a Bruker Avance400. Photoelectrochemical measurements were carried out in a conventional three-electrode, single-compartment quartz cell on an electrochemical station (CHI 660D). The Ti^{3+}/TiO_2 electrodes with an active area of ca. 1 cm^2 were served as working electrode. For the working electrodes, 20 mg of the photocatalyst was ground with 0.01 g polyethylene glycol (PEG, molecular weight 20000) and 0.5 mL ethanol to make a slurry. Afterward, the slurry was coated onto a 3 cm*1 cm F-doped SnO_2-coated glass (FTO glass) electrode by the doctor blade method, with an active area of ca.1 cm^2. The electrodes were calcined at 200 ^{o}C for 3 h in a ceramic plate heater. All the electrodes used had a similar thickness (1.0-1.5mm). The counter electrode and the reference electrode were platinum sheet and saturated calomel electrode (SCE), respectively. A bias voltage of 0.5 V was utilized for driven the photo-generated electrons transfer from working electrode to platinum electrode. A 300 W Xe lamp with an ultraviolet filter ($\lambda > 420$ nm) was used as visible light source and positioned 10 cm away from the photo-electrochemical cell. A 0.5 mol/L Na_2SO_4 aqueous solution was used as the electrolyte. The transient photocurrent curves were measured under an applied bias of 0.5 V.

Activity test

1. Photocatalytic degradation. Briefly, 50 mg photocatalyst was dispersed in 50 mL Rhodamine B (RhB) aqueous solution (10 mg/L) and stirred in dark for 1 h for reaching the adsorption/desorption equilibrium. During photocatalysis, a 300 W Xenon lamp (PLS-SXE300CUV, UV percent = 5.2 %) was used to simulate solar lights. For achieving visible lights induced photocatalysis, all the lights with wavelength shorter than 420 nm were cut-off by a filter to get visible-lights. After reaction for 4 h under 1000 r/min stirring, 2.0 mL suspension was sampled into plastic tube and centrifuged to remove the photocatalyst particles. The concentration of remained RhB was determined by UV-visible spectrophotometer analysis at its characteristic wavelength of 554 nm, from which the photocatalytic degradation yield was obtained by comparing with the initial RhB concentration. For comparison, the photocatalytic degradation of RhB was also conducted by using a 300 W Xenon lamp without removing UV lights with wavelength shorter than 420 nm. Meanwhile, 8 LED lamps (light intensity = 3.5 mW/cm^2, UVEC-4 Ⅱ devices purchased from Shenzhen Lamplic Science Co., Ltd) with single wavelength of 420 nm were used instead of a 300 W Xenon lamp for driving photocatalytic degradation of

RhB. In addition, photocatalytic degradation of aniline in aqueous solution (10 mg/L) was also carried out by using visible lights with wavelength longer than 420 nm from a 300 W Xenon lamp. The concentration of remained aniline was determined by UV-visible spectrophotometer analysis at its characteristic wavelength of 230 nm, from which the photocatalytic degradation yield was obtained by comparing with the initial aniline concentration.

2. Photocatalytic H_2 generation. Hydrogen production by photocatalytic water-splitting was carried out at room temperature in a three flat-bottomed flask reaction cell. Typically, 50 mg photocatalyst doped with 1 wt% Pt through *in situ* photo-reduction of H_2PtCl_6 was dispersed in 80 mL aqueous solution containing 20 mL methanol as the sacrificial reagent under ultrasonication. A 300 W Xenon lamp was used as simulated solar lights, positioned 1 cm away from the reactor. The evolved H_2 amount was determined using a gas chromatograph (Shanghai Ke Chuang, GC-9800, TCD, N_2 carrier and 5 A molecular sieve columns).

Results and discussion:

As shown in Fig. 1a, the as-received Ti^{3+}/TiO_2 sample was present in black powders. TGA analysis (Fig. S1) displayed no significant weight loss until 450 ^oC, indicating the absence of organic species. The XRD pattern in Fig. 1b demonstrated the single-crystal anatase TiO_2 (JCDPS 21-1272) in about 20-30 μm regular particles (see the SEM image in Fig. 1c). HRTEM (Fig. 1d) shows that the as-prepared TiO_2 nanocrystals were covered with disordered layers. Both HRTEM and the SAED images (Fig. 1d) further confirmed the single-crystal anatase phase. Based on the SAED, it can be defined that the as-prepared samples had the exposed facets which were {001} and {101} combined with Fig 1c.In addition, the SAED in Fig. 1(d) shows the (002) and (011) atomic planes with a lattice spacing of 0.189 nm and 0.352 nm respectively. The XRD patterns (Fig. S2) further confirmed that the as-prepared black Ti^{3+}/TiO_2 remained anatase phase until the calcination temperature reaching 600 ^oC and then totally transferred into rutile phase at 700 ^oC, showing excellent thermal stability against phase change.

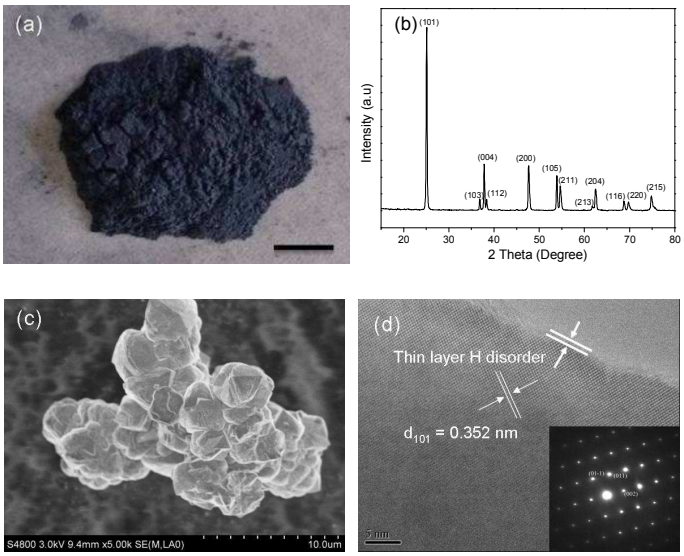

Figure 1. (a) Digital picture, (b) XRD pattern, (c) SEM image, and (d) HRTEM image of the as-prepared black Ti^{3+}/TiO_2. The inset is the SAED image. Scale bar in (a): 10 mm.

As shown in Fig. 2, the ^1H NMR spectra revealed that, besides a weaker signal at 4.7 ppm indicative of the H at bridging sites observed in pure while TiO_2[26, 27], the black Ti^{3+}/TiO_2 displayed three additional strong signals at -0.18 ppm, 0.97 ppm and 1.90 ppm, corresponding to the terminal and internal hydroxyl groups of anatase TiO_2[26]. These groups were associated with the H located in the disordered surface layer of the black Ti^{3+}/TiO_2,[28] which could be completely removed after being calcined in air at 700 ^oC.

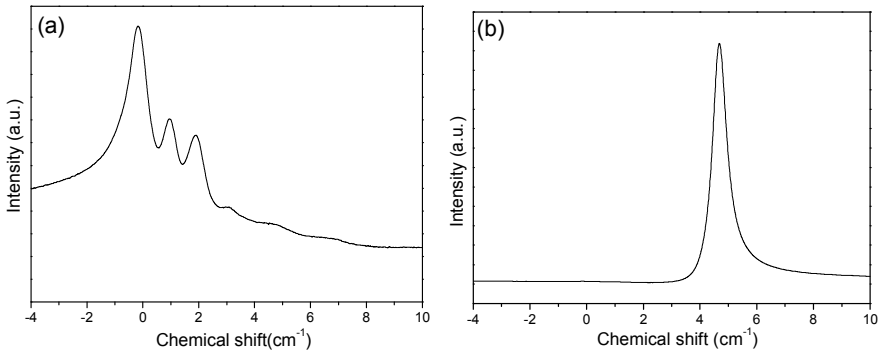

Figure 2. ^1H NMR spectra of black Ti^{3+}/TiO_2 (a) and white TiO_2 obtained by calcining Ti^{3+}/TiO_2 at 700 ^oC (b).

Scheme 1 briefly illustrates the formation of black Ti^{3+}/TiO_2 by the reaction between the Ti

foil and the ionic liquids (ILs) under ionothermal conditions. During the reaction, the fluoride enriched ionic liquid (IL) could dissolve Ti foil gradually. The SEM images and XRD patterns (Fig. S3) revealed that very little ionic liquid (0.5 mL) could dissolve only the outer surface of Ti foil, leading to a thin anatase TiO_2 film on the Ti foil. The Ti foil could be severely dissolved into bumps in the presence of 1.0 mL IL, corresponding to the formation of black Ti^{3+}/TiO_2 either in the solution or on the surface of Ti bumps. Further increase of IL to 2.0 mL resulted in complete dissolve of Ti foil, leading to the pure black Ti^{3+}/TiO_2 in regular particles with an average size about 20~30 μm in Fig. 1c. During the dissolving process of Ti foil under ionothermal conditions, H_2 gas could be produced *via* the reduction of H^+ from acetic acid by metal Ti, which could be confirmed by the following controlled experiment. After ionothermal treatment of Ti foil for 24 h, the autoclave was opened in a self-made glove box (volume = 60 L) filled with high purity N_2. 0.5 mL gas was sampled and analyzed by GC (GC9800, Shanghai Ke Chuang Chromatograph Instruments Co. Ltd, China, TCD, with nitrogen as a carrier gas and 5 A molecular sieve columns), which clearly displayed a typical H_2 peak as observed by introducing H_2 into autoclave before ionothermal process (see Fig. S4), indicating the H_2 generation during Ti foil dissolving under ionothermal conditions.

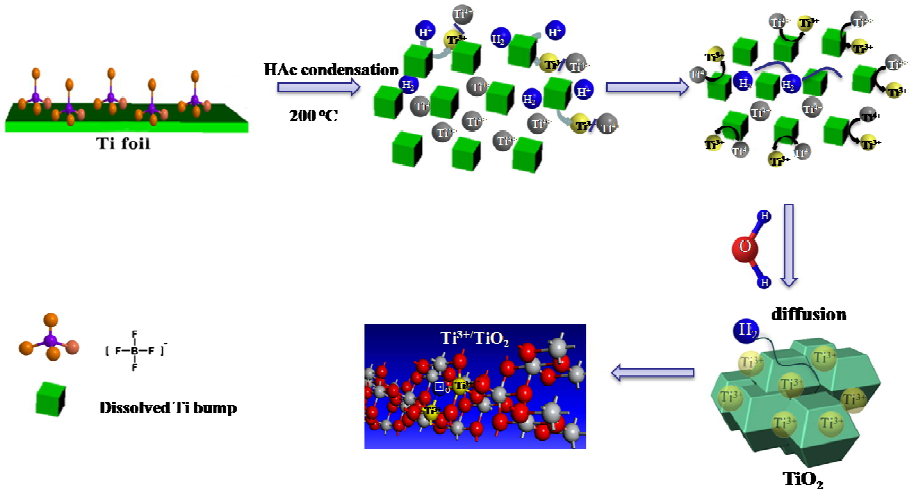

Scheme 1. The formation process of the black Ti^{3+}/TiO_2 under ionothermal conditions.

Based on the above results, it is reasonable that the black Ti^{3+}/TiO_2 formation process may include the following 4 steps. 1) Ti foil reacted with the H^+ ions resulted from ionization of HAc to form Ti^{4+}/Ti^{3+} ions and hydrogen gas in which the concentration of Ti^{4+} ions could be much

higher than that of Ti^{3+} ions. 2) Some of the formed Ti^{4+} ions will be further reduced to Ti^{3+} ions by the metal Ti[29]. 3) The Ti^{4+} and Ti^{3+} ions underwent ionothermal hydrolysis owing to the presence of trace H_2O resulted from the dehydration of acetic acid. The LC-MS patterns (Fig. S5) clearly displayed the presence of acetic anhydride in the ionic liquid obtained after ionothermal treatment of Ti foil for 24 h. During ionothermal hydrolysis process, Ti^{4+} transformed into anatase TiO_2 and Ti^{3+} ions may corporate into TiO_2 lattice. 4) The *in-situ* generated H_2 could be strongly adsorbed onto the TiO_2 surface and dissociated into H atom to form H-TiO_{2-x} disordered layer. Some important reactions involved the whole process are listed as follows.

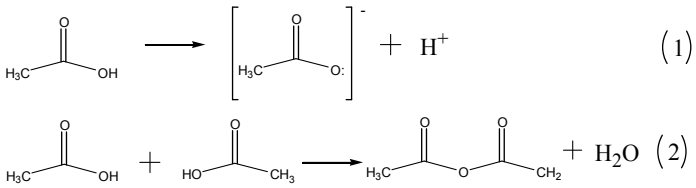

$$H^+ + Ti \longrightarrow Ti^{3+}/Ti^{4+} + H_2 \quad (3)$$

$$Ti^{4+} + Ti \longrightarrow Ti^{3+} \quad (4)$$

$$Ti^{4+} + H_2O \longrightarrow TiO_2 \quad (5)$$

$$TiO_2 + H_2 \xrightarrow{diffusion} H\text{-}TiO_2 \quad (6)$$

The EPR spectra (Fig. S6) of the as-prepared black Ti^{3+}/TiO_2 displayed strong signals in the *g* range from 1.99 to 1.94 which could be remained after being calcined at the temperature up to 500 ^oC, confirming the presence of Ti^{3+} species.[30] After being calcined at 700 ^oC, nearly all the Ti^{3+} species were oxidized into pure TiO_2. The XPS spectra in Ti 2p level (Fig. S7) also demonstrated the co-existence Ti^{3+} (457.5 eV $2P_{3/2}$ and 463.7 eV $2P_{1/2}$) and Ti^{4+} (459.1 eV $2P_{3/2}$ and 464.7 eV $2P_{1/2}$)[31] in the black Ti^{3+}/TiO_2 when it was calcined below 500 ^oC and completely transformed into pure TiO_2 after being calcined at 700 ^oC. A semi-quantitative analysis of Ti^{3+}/Ti^{4+} molar ratio could be calculated based on the XPS spectra (Table S1). The fresh black Ti^{3+}/TiO_2 displayed a Ti^{3+}/Ti^{4+} molar ratio of 0.162, which quickly decreased after calcinations at elevated temperatures due to the oxidation of Ti^{3+}. From 300 ^oC to 500 ^oC, the Ti^{3+}/Ti^{4+} molar ratio decreased from 0.128 to 0.101. After being calcined at 700 ^oC, the Ti^{3+}/Ti^{4+} ratio decreased to about 0, indicating all of the Ti^{3+} ions were transferred to Ti^{4+} ions owing to the oxidation effect of O_2. In addition, the Raman spectra also confirmed the presence of oxygen vacancies. As well known, the pure anatase TiO_2 displays 6 typical peaks around 144, 197, 639, 399, 519, and 513

cm^{-1}, corresponding to the $E_{g(1)}$, $E_{g(2)}$, $E_{g(3)}$, $B1_{g(1)}$, $B1_{g(2)}$ and A_{1g} modes[32,33]. As shown in Fig. 3, the fresh black Ti^{3+}/TiO_2 exhibited a principal peak around 157.0 cm^{-1} characteristic of oxygen vacancies. Calcining at 300 ^oC had no significant influence on the Raman spectra. Increase the calcination temperature to 500 ^oC resulted in a negative shift of the principal peak from 157.0 cm^{-1} to 151.3 cm^{-1}. Further increasing the calcining temperature to 700 ^oC led to the formation of anatase TiO_2 to rutile TiO_2 as indicated in both Fig. 3a and aforementioned XRD pattern (Fig. S2), together with the continued negative shift to about 147.1 cm^{-1}, implying a great decrease in oxygen vacancies [34]. These results clearly demonstrated that the oxygen vacancies produced due to the replacement of Ti^{4+} ions with Ti^{3+} ions in TiO_2 lattice (see the following equation)[35] and the number of oxygen vacancies decreased gradually during calcinations at elevated temperatures due to the oxidation of Ti^{3+} into TiO_2.

$$4Ti^{4+} + O^{2-} \rightarrow 4Ti^{4+} + 2e^-/\square + 0.5\ O_2 \rightarrow 2Ti^{4+} + 2Ti^{3+} + \square + 0.5\ O_2$$

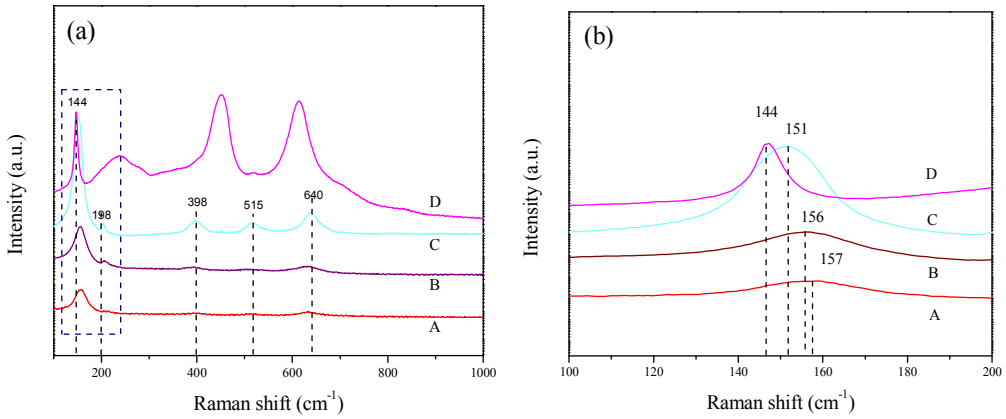

Figure 3. Raman spectra (a) and the corresponding enlarged Raman spectra from 100 to 200 cm^{-1} (b) of the as-prepared black Ti^{3+}/TiO_2 before (A) and after being calcined at elevated temperatures 300 ^oC (B), 500 ^oC (C), 700 ^oC (D).

The UV-Vis DRS spectra in Fig. 4 revealed that the black Ti^{3+}/TiO_2 displayed an extended absorption band up to ca. 800 nm. And the calcined samples had the broad peak at ca. 680 nm which is consistent with the color change of the samples. The broad peak at 680 nm might be due to forming oxygen vacancy energy level in the bandgap. In the illumination, the photo-generated electron was graded transition. Calcining the black Ti^{3+}/TiO_2 samples at elevated temperatures resulted in the gradual blue-shift of the light absorbance[21]. The black Ti^{3+}/TiO_2 and calcining at

different temperature samples all had the decreasing optical bandgap with the color-dependence. Thus, the visible light absorbance of the black Ti^{3+}/TiO_2 could be mainly ascribed to the existence of defect states in TiO_2 band gap owing to the presence of Ti^{3+}-dopants and oxygen vacancies[36] in accordance with the XPS analysis.

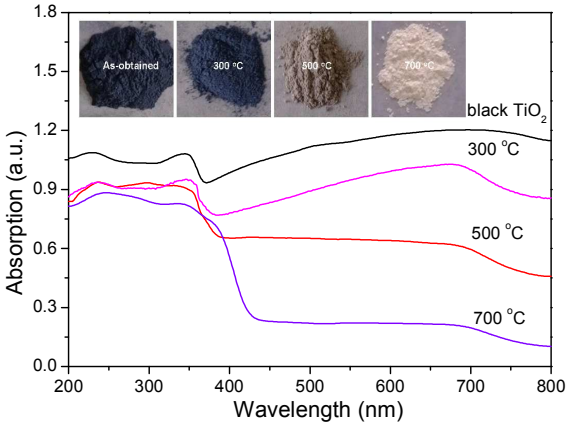

Figure 4. The UV-vis diffuses reflectance spectra (DRS) and the digital photos of the as-prepared Ti^{3+}/TiO_2 before and after being calcined at elevated temperatures.

Based on 1*1*2 and 2*2*1 anatase TiO_2 super cells, the electronic structure of the black Ti^{3+}/TiO_2 could be calculated by using CASTEP model[37 38]. To calculate the concentration of oxygen vacancy, one O atom is removed from each super cell. During the calculation, a suitable plane-wave basis set with an energy cutoff of 408 eV was selected for the ultra-soft pseudopotential with Perdew-Burke-Ernzerhof exchange correlations. Brillouin-zone integration is computed with k points in a Monkhorst- Pack (10, 10, 5) grid. As known, the H disorder-adsorbed on the surface of black Ti^{3+}/TiO_2 could form a mid-gap state. It can form a continuum extending to or overlapping with the conduction band edge, named band tail states[24]. It is found that the Fermi level is much closer to the conduction band tail states at high oxygen vacancy concentration (see Fig. S8). Thus, it is reasonable that the high concentration of oxygen vacancy may break the selection rule for indirect transitions, leading to an enhanced absorption for photon energy below the direct band gap,[39] in good accordance with the UV-vis DRS spectra (see Fig. 4). Based on above calculation, a scheme of the structure and density of states (DOS) is illustrated in Fig. 5. The gap states form a mini-band below the conduction band edge. It could be seen that the conduction band edge will turn broad at enhanced oxygen vacancy concentration. Meanwhile, the band of defect-states resulted from oxygen vacancy is very close to the conduction band edge,

allowing photo-generated electrons to easily exchange between two bands. Under visible-light irradiation, the electron from the valence band (VB) can easily transfer to the oxygen vacancy level existing in the band gap. Therefore, the electronic transfer from both valence band and oxygen vacancy level localized states to tailed conduction band (CB).

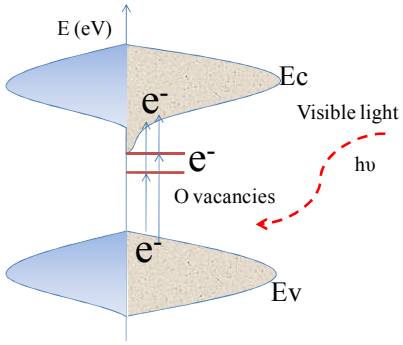

Figure 5. The scheme of the structure and density of states (DOS) for pure TiO_2 (left) and black Ti^{3+}/TiO_2 (right), together with conduction and valence levels of bulk semiconductor (Ec and Ev).

As shown in Fig. 6a, all the Ti^{3+}/TiO_2 samples display PLS peaks at around 560 nm regardless of the calcination temperature. The intensity increased with the enhanced calcination temperature, indicating the increased photoelectron-hole recombination rate,[40] since the reduced concentration of Ti^{3+}-dopants caused the decrease in oxygen vacancies, which could capture photoelectrons and thu, inhibit the photoelectron-hole recombination. Meanwhile, as shown in Fig. 6b, the black Ti^{3+}/TiO_2 exhibited strong photocurrent response. Calcinations of the black Ti^{3+}/TiO_2 at elevated temperatures in air resulted in significant decrease in photocurrent response, which could be attributed to both the decrease in absorbance for visible lights (see Fig. 4) and the increase of photoelectron-hole recombination rate (see Fig. 6a) [41] due to the reduced concentration of Ti^{3+}-dopants and oxygen vacancies.

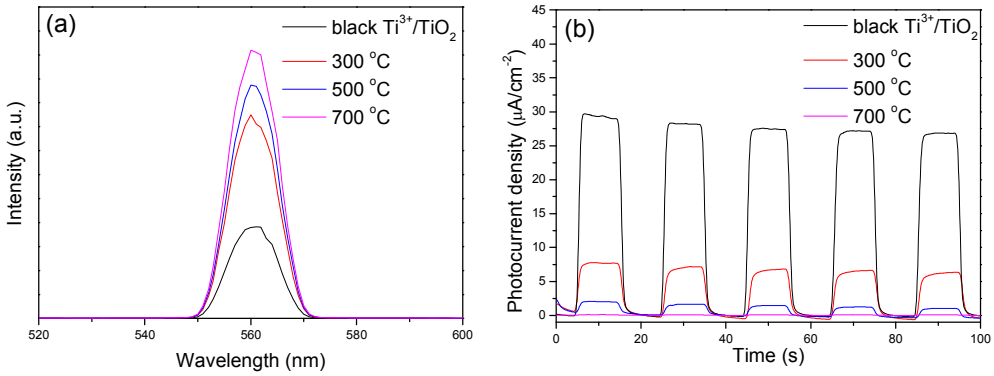

Figure 6. (a) PLS spectra (excited by 280 nm) and (b) the visible lights (λ > 420 nm) induced photocurrent of the black Ti^{3+}/TiO_2 before and after being calcined at elevated temperatures.

As shown in Fig. 7a, the as-prepared black Ti^{3+}/TiO_2 exhibited relatively high activity during visible light driven photocatalytic degradation of RhB. The photocatalytic activity decreased gradually after being calcined at elevated temperature from 300 °C to 700 °C, which could mainly be attributed to the decrease in both the Ti^{3+} content and the oxygen vacancy number due to the oxidation in air at high temperature. The white TiO_2 obtained at 700 °C displays no significant activity, obviously due to the complete transformation of Ti^{3+} into TiO_2 and the total disappearance of oxygen vacancies, taking into account that either the pure anatase or the pure rutile TiO_2 could not be activated by visible-light due to their big energy band gaps[39]. As shown in Fig. 7b, the as-prepared black Ti^{3+}/TiO_2 also exhibited strong durability and could be used for 4 times without any deactivation. For excluding the self-sensitization effect of RhB at 554 nm, the 8 LED lamps with wavelength of 420 nm and light intensity of 3.5 mW/cm^2 were employed as a single-wavelength light source for driving the photocatalytic reaction. As shown in Fig. 7c, 40 % RhB removal rate was obtained after reaction for 4 h over the fresh black Ti^{3+}/TiO_2, which was similar to that obtained under Xenon light irradiation with wavelength longer than 420 nm. Meanwhile, Fig. 7d also demonstrated the efficient degradation of colorless aniline under visible light irradiation (λ > 420 nm, Xenon lamp). It was also noted that only a about 19 % removal rate was obtained *via* choosing phenol as another colorless organic pollutants. For better comparison, commercial P25 was also utilized as standard. P25 exhibited an 79.7 % removal rate of RhB under under Xenon light irradiation with wavelength longer than 420 nm, however its activity was greatly decreased to very low (about 5 % removal rate) under 420 nm LED irradiation while

keeping other conditions unchanged. 79.7 % removal rate of RhB for P25 is attributed to its strong RhB-sensitization effect, which was evidenced by our earlier reported work.[42] To the case of 420 nm LED irradiation, the RhB-sensitization effect was avoided with the formation of a negative activity for P25. All these results indicated that the present visible-light induced photocatalytic degradation was attributed to the intrinsic properties of the black Ti^{3+}/TiO_2 rather than the photosensitizing effect.

It was also found that the RhB degradation yield greatly enhanced up to 91% even after reaction for 3 h by using a 300 W Xenon lamp irradiation without removing UV lights (see Fig. S9), implying that the UV lights in the Xenon lamp could more effectively activate the black Ti^{3+}/TiO_2, which could also be observed for the black Ti^{3+}/TiO_2 after being calcined at elevated temperatures. Moreover, it was found that the concentrations of both the Ti^{3+}-dopants and oxygen vacancies had very little influence on the photocatalytic activity induced by UV lights since no much change in RhB degradation yield was observed even after calcination of the black Ti^{3+}/TiO_2 up to 500 ^{o}C. From those results, we could guess that the Ti^{3+}-dopants and oxygen vacancies promoted photocatalytic activity mainly *via* generating intermediate energy levels to narrow the energy band gap rather than *via* capturing photoelectrons to reduce photoelectron-hole recombination. To our surprise, the black Ti^{3+}/TiO_2 after being calcined at 700 ^{o}C exhibited slightly higher activity than the fresh sample, which could be ascribed to the formation rutile/anatase TiO_2 heterojunctions, allowing a fast photo-generated electron transfer rate.[43]

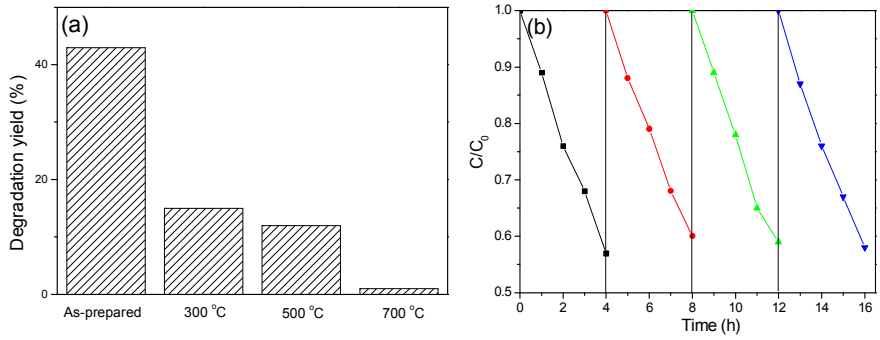

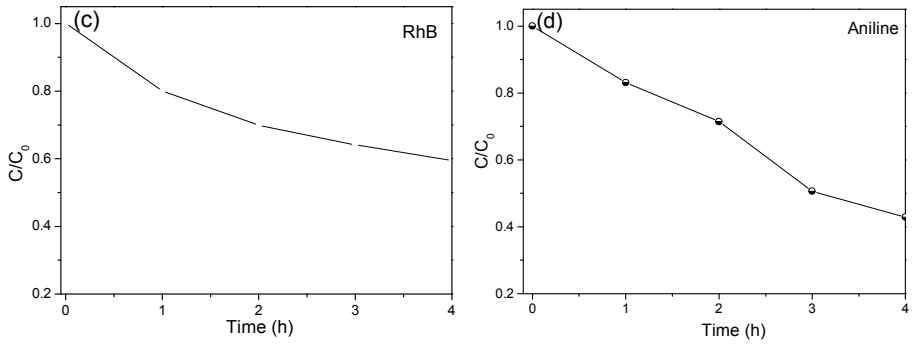

Figure 7. (a) Photocatalytic activities of the black Ti^{3+}/TiO_2 before and after being calcined at elevated temperature and (b) Recycling test of the fresh black Ti^{3+}/TiO_2 for RhB degradation in aqueous solution under visible-light (λ > 420 nm) irradiation. Reaction conditions: 50 mg photocatalyst, 50 mL RhB aqueous solution (10 mg/L), room temperature, 4 h. (c) The photocatalytic degradation of RhB with the fresh black Ti^{3+}/TiO_2 under 8 LED lamps (each light intensity = 3.5 mW/cm^2) illumination. Other reactions are the same as those in Figure 7(a). (d) The photocatalytic degradation of aniline (10 mg/L) with the fresh black Ti^{3+}/TiO_2 under visible-light illumination (λ > 420 nm). Other reactions are the same as those in Figure 7(a).

To clarify the mechanism of the photocatalytic degradation of aqueous RhB in the presence of the as-prepared black Ti^{3+}/TiO_2, we introduced various reactive species scavengers, including sodium oxalate (10 mg), isopropanol (1.0 mL), $AgNO_3$ (10 mg), and nitrogen gas, to the photocatalytic reaction system for investigating the effect of holes (h_{vb}^+), hydroxyl radicals (·OH), photo-generated electrons (e^-) and oxygen anion molecules ($\cdot O^{2-}$) on the removal efficiency of RhB under visible-light irradiation. As shown in Figure 8, it was found that the addition of $AgNO_3$, as the electron scavenger, had only a weak influence on the photocatalytic degradation of RhB. This indicates that the photogenerated electrons are not the key for degrading RhB. As known, the formation of superoxide anions ($\cdot O_2^-$), an important active radical for photocatalytic reactions, resulted from the reaction between the dissolved oxygen in the reaction system and photogenerated electrons. Upon purging with nitrogen gas, oxygen molecules could be expelled from the reaction system, inhibiting the formation of superoxide anions. The removal rate of RhB was also decreased slightly. This indicates that $\cdot O_2^-$ is not the key factor affecting the photocatalytic performance of the black Ti^{3+}/TiO_2. In addition, when adding isopropanol (IPA) to minimize the formation of ·OH radicals, it was found that the addition of isopropanol greatly reduced the photodegradation rate of RhB from 43 % to about 15 % in the black Ti^{3+}/TiO_2. The ·OH radicals were further detected by a terephthalic acid photoluminescence probing. The

fluorescence intensity was found to increase steadily with irradiation time (Fig. S10a), indicating that hydroxyl radicals can be generated in the black Ti^{3+}/TiO_2 system under visible light ($\lambda > 420$ nm) irradiation. The ESR spin-trap technique (with DMPO) was also further chosen to probe the hydroxyl radicals generated on the surface of the black Ti^{3+}/TiO_2. As shown in Fig. S10b, four characteristic peaks of DMPO-•OH were obviously observed in the suspension of black Ti^{3+}/TiO_2[44]. This is consisted with the description of by using the terephthalic acid to probe hydroxyl radicals in PL experiment.

Moreover, a significant 72 % decrease in the photocatalytic activity was attributed to the addition of sodium oxalate ($Na_2C_2O_4$) for trapping photogenerated holes (h_{vb}^+). These results imply that the degradation of RhB by the black Ti^{3+}/TiO_2 photocatalyst seemed to be ascribed to a dual mechanism involving both surface h_{vb}^+ and ·OH radicals. To the case of the sample, the black Ti^{3+}/TiO_2, the absorptive intensity of RhB at a wavelength of 554 nm gradually decreases and the absorption band shifts to shorter wavelengths at 540 nm as shown in Figure S11. Furthermore, no new absorption bands appear in either the visible or the UV region. This suggests the complete photocatalytic decomposition of RhB during the reaction on black Ti^{3+}/TiO_2 sample.

Therefore, it can be concluded that the photo-oxidation mechanism occurring on the surface of the black Ti^{3+}/TiO_2 may involve the direct reaction of the organic chemical (dye) with surface h_{vb}^+ and indirect reaction with ·OH radicals, or a dual mechanism involving both surface h_{vb}^+ and ·OH radicals (equation 7).

$$h_{vb}^+/{}^{\cdot}OH + \text{dye (RhB)} \rightarrow CO_2 + H_2O \qquad (7)$$

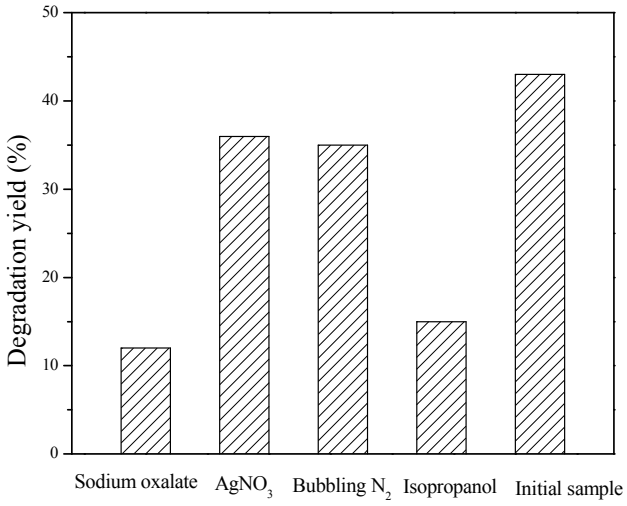

Figure 8. Effect of Effect of sodium oxalate ($Na_2C_2O_4$), $AgNO_3$, N_2 and isopropanol on the photocatalytic performance of black Ti^{3+}/TiO_2 for degrading RhB (10 mg/L) in 4 hours under visible light.

Besides the high activity in photocatalytic degradation of organic pollutants, such a black Ti^{3+}/TiO_2 could also be employed in photocatalytic water-splitting for H_2 evolution under simulated solar lights irradiation (a 300 W Xenon lamp without removing UV lights) *via* choosing methanol as the sacrificial reagent. As shown in Table 1, the as-prepared black Ti^{3+}/TiO_2 displayed similar activity to both the S-doped TiO_2[25] and the I-doped TiO_2[45], which were widely recognized as highly active visible photocatalysts for H_2 evolution *via* water splitting. Meanwhile, its H_2 evolution activity (0.26 mmol/h*m^2) was about two times of that of P25, suggesting the as-preapred black Ti^{3+}/TiO_2 had excellent intrinsic activity.

Table 1. H_2 evolution rates over different photocatalysts irradiated with simulated solar lights[a]

Photocatalyst	H_2 evolution rate (mmol/h·m^2)
Black Ti^{3+}/TiO_2	0.26
S-doped TiO_2	0.29
I-doped TiO_2	0.25
P25	0.13

[a]Reaction conditions: 50 mg photocatalyst doped with 1 wt% Pt, 80 mL aqueous solution containing 20 mL methanol, a 300 W Xenon lamp located at 10 cm away from the reaction system, room temperature.

Conclusions

This work developed a facile strategy to prepare black Ti^{3+}-doped singe-crystal anatase TiO_2 (Ti^{3+}/TiO_2) in one-pot by treating Ti in an ionic liquid containing LiAc and HAc under mild ionothermal conditions. This Ti^{3+}/TiO_2 contained high-contents of Ti^{3+}-dopants incorporated into TiO_2 lattice and oxygen vacancies, which facilitated the activation by visible lights and also reduced the photoelectron-hole recombination. It exhibited high activity in both photocatalytic degradation of organic pollutants and H_2 generation under irradiation with visible lights and/or simulated solar lights.

Supporting Information

Ti^{3+}/Ti^{4+} and oxygen vacancy molar percentages, O2s XPS spectra of black TiO_2, FESEM images of the as-prepared samples via choosing various amount of ionic liquids (1-methyl-imidazolium tetrafluoroborate), TGA curve of the black TiO_2 sample under an air flow, the detection of hydrogen produced in the ionothermal treatment process of Ti foil by the gas chromatograph measurement, XRD patterns for as-prepared samples with different calcining temperature, EPR spectra, Ti 2p XPS spectra of various samples, calculated density of electronic states for anatase TiO_2, the photocatalytic degradation of RhB with the samples calcined at various temperature in air under Xenon lamp illumination. This material is available free of charge via the Internet at http://pubs.acs.org.

Acknowledgements

This work was supported by National Natural Science Foundation of China (21207090, 21477079, 21261140333, 21237003), Doctoral program of Higher Education (20123127120009), Shanghai Government (11SG42, 11ZR1426300, 14ZR1430900, IRT1269), and by a scheme administrated by Shanghai Normal University (SK201104, DXL122, and S30406).

REFERENCE

1. A. O. Kondrakov, A. N. Ignatev, F. H. Frimmel, S. Bräse, H. Horn, A. I. Revelsky, *Appl. Catal. B*: *Environ.*, 2014, **160-161**, 106-114.

2. J. Ran, J. Zhang, J. Yu, M. Jaroniec, S. Z. Qiao, *Chem. Soc. Rev.*, 2014, DOI: 10.1039/C3CS60425J.

3. M. R. Hoffmann, S. T. Martin, W. Choi and D. W. Bahnemann, *Chem. Rev.*, 1995, **95,** 69-96.

4 A. Fujishima and K. Honda, *Nature*, 1972*,* **238,** 37-38.

5 R. Long, English and N. J., *Phys. Rev. B.*, 2011, **83,** 155209-155214.

6 G. Liu, L. C. Yin, J. Wang, P. Niu, C. Zhen, Y. Xie and H. M. Cheng, *Energ. Environ. Sci.*, 2012*,* **5**, 9603-9610.

7. W. Zhou, T. Li, J. Wang, Y. Qu, K. Pan, Y. Xie, G. Tian, L. Wang, Z. Ren, B. Jiang, H. Fu, *Nano. Res.*, 2014, **7**, 731-742.

8. G. Li, D. Zhang, J. C. Yu, *Phys. Chem. Chem. Phys.*, 2009, **11**, 3775-3782.

9. J. Hong, Y. Wang, Y. Wang, W. Zhang, R. Xu, *ChemSusChem,* 2013, **6**, 2263-2268.

10. T. Zhou, Y. Du, A. Borgna, J. Hong, Y. Wang, J. Han, W. Zhang, R. Xu, *Energ. Environ. Sci.*, 2013, **6**, 3229-3234.

11. G. Nagaraju, T. N. Ravishankar, K. Manjunatha, S. Sarkar, H. Nagabhushana, R. Goncalves, J. Dupont, *Mater. Lett.*, 2013, **109**, 27-30.

12. D. Zhang, M. Wen, B. Jiang, G. Li, J. C. Yu, *J. Hazard. Mater.*, 2012, **211-212**, 104-111;

13. X. Wang, Q. Wang, F. Li, W. Yang, Y. Zhao, Y. Hao, S. Liu, *Chem. Eng. J*, 2013, **234**, 361-371.

14. M. Liu, L. Piao, W. Lu, S. Ju, L. Zhao, C. Zhou, H. Li, W. Wang, *Nanoscale*, 2010, **2**, 1115-1117.

15. L. Liu, Z. Liu, A. Liu, X. Gu, C. Ge, F. Gao, L. Dong, *ChemSusChem*, 2014, **7**, 618-626.

16. L.-L. T. Wee-Jun Ong, Siang-Piao Chai, Siek-Ting Yong and Abdul Rahman Mohamed, *Nano Res.*, 2014**,** DOI: 10.1007/s12274-014-0514-z.

17. D. Zhang, G. Li, X. Yang, J. C. Yu, *Chem. Commun.*,2009, 4381-4383.

18. O. Lamiel-Garcia, S. Tosoni, F. Illas, *J. Phy. Chem. C*, 2014, **118**, 13667-13673.

19. W. J. Ong, L. L. Tan, S. P. Chai, S. T. Yong, A. R. Mohamed, *Nanoscale,* 2014, **6**, 1946-2008.

20. W. J. Ong, L. L. Tan, S. P. Chai, S. T. Yong, A. R. Mohamed, *ChemSusChem*, 2014, **7**, 690-719.

21. Z. Sun, H. Tan, Z. Zhao, M. Niu, C. Mao, D. Cao, D. Cheng and P. Feng, *Nanoscale*, 2014, DOI: 10.1039/C4NR02677B.

22 F. Zuo, L. Wang, T. Wu, Z. Zhang, D. Borchardt and P. Feng, *J. Am. Chem. Soc.*, 2010, **132**, 11856-11857.

23 A. Naldoni, M. Allieta, S. Santangelo, M. Marelli, F. Fabbri, S. Cappelli, C. L. Bianchi, R. Psaro, and V. Dal Santo, *J. Am. Chem. Soc.*, 2012, **134**, 7600-7603.

24 X. Chen, L. Liu, P. Y. Yu and S. S. Mao, *Science*, 2011, **331**,746-750.

25 C. Yang, Z. Wang, T. Lin, H. Yin, X. Lü, D. Wan, T. Xu, C. Zheng, J. Lin, F. Huang, X. Xie, and M. Jiang, *J. Am. Chem. Soc.*, 2013, **135**, 17831-17838.

26 M. Crocker, R. H. M. Herold, A. E. Wilson, M. Mackay, C. A. Emeis and A. M. Hoogendoorn, *J. Chem. Soc. Faraday Trans.,*1996, **92**, 2791-2798.

27 Z. Wang, C. Yang, T. Lin, H. Yin, P. Chen, D. Wan, F. Xu, F. Huang, J. Lin, X. Xie and M. Jiang, *Adv. Funct. Mater.*, 2013, **23**, 5444-5450.

28 X. B. Chen, L. Liu, Z. Liu, M. A. Marcus, W. C. Wang, N. A. Oyler, M. E. Grass, B. H. Mao, P. A. Glans, P. Y. Yu, J. H. Guo and S. S. Mao, *Sci. Rep.*, 2013, **3,** 1510.

29. R. Liu and A. Sen, *J. Am. Chem. Soc.*, 2012**, 134**, 17505-17512.

30 J. C. Conesa and J. Soria, *J. Phys.Chem.*, 1982, **86**, 1392-1395.

31 G. Liu, H. G. Yang, X. W. Wang, L. N. Cheng, H. F. Lu, L. Z. Wang, G. Q. Lu and H. M. Cheng, *J. Phys. Chem. C*, 2009, **113**, 21784-21788.

32. X. Pan, M.-Q. Yang, X. Fu, N. Zhang and Y.-J. Xu,. *Nanoscale,* 2013, **5**, 3601-3614.

33 T. Ohsaka, F. Izumi and Y. Fujiki, *J Raman Spectrosc.*, 1978, **7**, 321-324.

34 J. C.Parker and R. W. Siegel, *Appl Phys Lett*, 1990, **57**, 943-945.

35 X. D. Jiang, Y. P. Zhang, J. Jiang, Y. S. Rong, Y. C. Wang, Y. C. Wu and C. X. Pan, *J. Phys. Chem. C*, 2012, **116**, 22619-22624.

36 Y. H. Hu, *Angew. Chem. Int. Ed.*, 2012, **51**, 12410-12412.

37 J. P. B. Perdew and K. Ernzerhof, *Phys. Rev. Lett*., 1996, **77**, 3865–3868.

38 M. S. C. Accelrys, Inc. Accelry, San Diego, 2011.

39 J. Zhang, S. Yan, L. Fu, F. Wang, M. Q. Yuan, G. X. Luo, Q. Xu, X. Wang and C. Li, *Chinese J Catal.*, 2011, **32**, 983-991.

40 G. Li, L. Wu, F. Li, P. Xu, D. Zhang and H. X. Li, *Nanoscale*, 2013, **5**, 2118-2125.

41 Y. Zhang, P. Zhang, Y. N. Huo, D. Q. Zhang, G. S. Li and H. X. Li, *Appl. Catal. B*, 2012, **115**, 236-244.

42 G. S. Li, B. Jiang, S. N. Xiao, Z. C. Lian, D. Q. Zhang, J. C. Yu and H. X. Li, Environ. Sci. Process Impacts, 2014, 16, 1975-80.

43 H. Y. Tian, G. H. Zhao, Y. N. Zhang, Y. B. Wang and T. C. Cao, *Electrochim. Acta.*, 2013, **96**, 199-205.

44 W. Zhao, W. Ma, C. Chen, J. Zhao and Z. Shuai, J. Am. Chem. Soc., 2004, **126**, 4782-4783.

45 T. Lin, C. Yang, Z. Wang, H. Yin, X. Lu, F. Q. Huang, J. Lin, X. Xie and M. Jiang, *Energ. Environ. Sci.*, 2014, **7**, 967-972.